

# Material Point Method Simulation of Equal Channel Angular Pressing Involving Large Plastic Strain and Contact Through Sharp Corners

V. Lemiale<sup>1,2</sup>, J. Nairn<sup>3</sup> and A. Hurmane<sup>1</sup>

**Abstract:** We assessed the suitability of the Material Point Method (MPM) to simulate the equal channel angular pressing technique (ECAP). This severe plastic deformation process combines several interesting and challenging features in the context of numerical simulations, namely large displacements, large plastic deformations, as well as abrupt contact changes between the rigid tools and the work piece. Moreover, ECAP has been intensively studied, experimentally, numerically and theoretically, which makes it an ideal benchmark for testing MPM. Results from finite element analysis are also presented for comparison to MPM because this method is widely considered as a robust and reliable computational technique that has often been successfully applied to severe plastic deformation processes. In general, an excellent agreement is found in the predictions made by the two numerical methods. However, we found that to successfully simulate such processes with MPM, prior contact methods should to be replaced with a new contact algorithm. The new contact method is presented and should improve other MPM simulations with contact as well.

**Keywords:** Material Point Method, Finite element, Contact, Equal Channel Angular Pressing, Metal forming process.

## 1 Introduction

Severe Plastic Deformation (SPD) processes refer to metal forming processes in which ultra-fine grained metals are produced by subjecting a sample to very large plastic strains [Valiev and Langdon (2006)]. Numerical models of SPD processes have been proposed in the literature as a complementary tool to experiments for a better understanding of the mechanisms of strain-induced grain refinement [Kim

---

<sup>1</sup> CSIRO, Clayton, VIC, Australia

<sup>2</sup> Monash University, Clayton, VIC, Australia

<sup>3</sup> Oregon State University, Corvallis, OR, U.S.A

(2001);Baik, Estrin, Hellmig, Jeong, Brokmeier and Kim (2003)]. In prior simulations, the Finite Element Method (FEM) was the most widely used numerical approach. Due to the very nature of SPD processes, however, a large distortion of the finite element mesh is expected in many instances; this distortion strongly affects the numerical predictions. For instance, in the High Pressure Torsion (HPT) experiment - one of the most investigated SPD processes - deformed samples can experience plastic strains of up to a thousand percent [Zhilyaev and Langdon (2008)]. Consequently, only a limited number of simplified FE models have been proposed to simulate this process as well as other techniques involving extreme straining [Kim (2001);Lapovok, Pougis, Lemiale, Orlov, Tóth and Estrin (2010)].

In this context, alternative solutions to conventional FE approaches would be useful. The Material Point Method (MPM) appears to be a promising candidate because its formulation eliminates the problem of mesh distortion. Indeed, MPM may be seen as a hybrid approach between standard FE analysis and pure meshless methods. More precisely, in MPM an Eulerian mesh is used for the formulation of the discretized problem, while Lagrangian particles or material points are introduced to track the material deformation through their motion. The so-called Gauss points, commonly associated with finite elements for volume integration, are replaced in MPM by these Lagrangian particles. Because the MPM mesh (or background grid) does not deform, the main advantage of MPM over FEM lies in its ability to handle very large deformations.

The application of MPM to solid mechanics problems is relatively recent and is generally traced back to the early work by [Sulsky, Chen and Schreyer (1994); Sulsky, Zhou and Schreyer (1995)] in the mid 1990's. Since then, MPM has been applied to a wide range of applications and a number of modifications of the original formulation have been proposed. For example, in geosciences [Moresi, Dufour and Mühlhaus (2003);Moresi, Quenette, Lemiale, Mériaux, Appelbe and Mühlhaus (2007)] developed a finite element particle in cell method to study the lithospheric deformation coupled with the ductile mantle. MPM has shown potential advantages for problems involving large amounts of contact and for problems with explicit crack propagation. For example, MPM was used to simulate foam [Bardenhagena, Brydon and Guilkey (2005)] and wood compaction [Nairn (2006)] through cell well buckling and well into a densification regime. The extension of MPM to include explicit cracks with crack contact [Nairn (2003)] and imperfect interfaces [Nairn (2007)] is also finding new applications.

While the relevance of MPM to large strain engineering problems has been demonstrated [Wieckowski (2004)], few quantitative analyses have been reported to assess its accuracy in problems dealing with geometric, material and contact non linearity all at the same time. The treatment of complex contact conditions is available in

MPM [Bardenhagen, Guilkey, Roessig, Brackbill, Witzel and Foster (2001)], but has not been systematically investigated for contact between rigid tools and deformable bodies, especially when they involve significant changes in surface normals during the simulation. In this paper, the technique of Equal Channel Angular Pressing (ECAP) was chosen as a benchmark experiment to assess the suitability of MPM to simulate such processes. ECAP was selected for a number of reasons. First, along with the HPT experiment previously mentioned, ECAP has been one of the most thoroughly studied SPD processes and therefore a large collection of both experimental and numerical data are available in the literature. Second, ECAP represents one example of an SPD process for which accurate FE solutions exist thus enabling a direct quantitative comparison between the two approaches. Finally, the problem itself involves a number of difficulties, most notably the treatment of contact between tools and a deformable body along with deformation of the body through a sharp corner.

This paper is organized as follows. In section 2, the numerical modeling of ECAP by MPM is discussed. The process itself is first introduced then details are given on the formulation of MPM emphasizing on the treatment of contact at interfaces between rigid and deformable bodies. Most importantly, we found that MPM with conventional contact methods [Bardenhagen, Guilkey, Roessig, Brackbill, Witzel and Foster (2001)] did not perform well. We diagnosed the contact problems as mostly caused by the technique used to find the contacting-surface normal vectors. Some new contact methods were developed and found to greatly improve the ECAP simulations; this improvement is presented in section 2. This section concludes with the main features of the numerical models used throughout this work. In section 3 the mechanical properties of the material considered in the present study, namely pure copper with or without strain hardening, are discussed. Section 4 reports on the influence of some of the most important numerical parameters that were investigated. The plunger speed, the sensitivity to the spatial resolution and the importance of using an appropriate contact algorithm are all discussed. Finally, in section 5 a number of ECAP simulations are presented in which the MPM results were compared with both FEM results and with reports from the literature. It is shown that MPM with optimized contact methods is a valuable alternative to FEA for large strain problems, including the area of SPD processes.

## 2 Simulating ECAP with MPM

### 2.1 *The Equal Channel Angular Pressing (ECAP) technique*

ECAP belongs to the class of processes commonly referred to as severe plastic deformation (SPD) processes. It is one of the most commonly investigated SPD

technique. The objective of SPD processes is to apply large plastic strains to a specimen, thereby generating a large amount of defects such as dislocations within the bulk of the material, which will in turn serve as the basis for a new, significantly refined microstructures [Azushima, Kopp, Korhonen, Yang, Micari, Lahoti, Groche, Yanagimoto, Tsuji, Rosochowski and Yanagida (2008)]. Indeed, the dislocations generated by plastic deformation will rearrange in dislocation cell structures with further straining, a process which may be seen as the seed for the generation of new grains with sizes typically smaller than  $1 \mu\text{m}$  [Baik, Estrin, Hellmig, Jeong, Brokmeier and Kim (2003)].

A schematic diagram of ECAP is provided in Fig. 1.

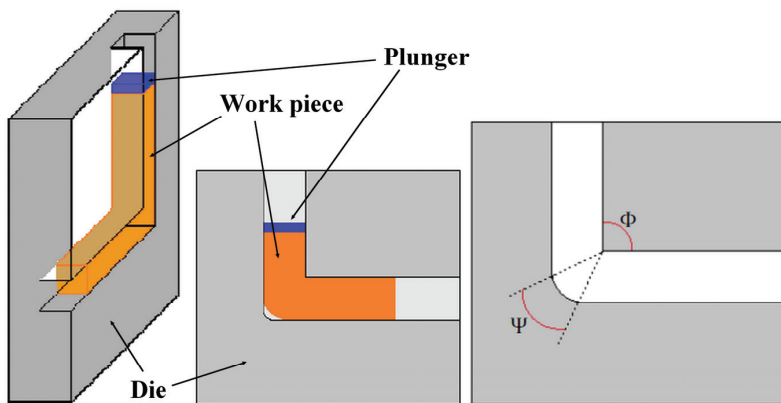


Figure 1: Schematic 3D representation (left) and 2D cross sections (middle and right) of a standard ECAP apparatus. The work piece is shown half way through the extrusion process. Some of the important process parameters, the inner angle  $\Phi$  and the outer angle  $\Psi$  are indicated on the right image.

The principle of ECAP is as follows. A billet is inserted in the ECAP die which is composed of an entry and an exit channel oriented at a pre-defined  $\Phi$  angle with each other. The billet is extruded through the exit channel by the action of a plunger and in doing so is subjected to large plastic strains, mostly in the form of simple shear loading (the validity of the simple shear approximation of course depends on the initial ECAP setup such as the two angles previously defined). After each pass, the amount of plastic strain experienced by the work piece is roughly 1, but again this is dependent on the initial ECAP setup.

ECAP is one of the few SPD processes for which a large number of numerical models exist [Baik, Estrin, Hellmig, Jeong, Brokmeier and Kim (2003);Figueiredo, Pin-

heiro, Aguilar, Modenesi and Cetlin (2006); Kim, Seo and Hong (2002); Xu, Zhao, Ren and Ma (2008)]. Most of these models are based on Lagrangian finite element analysis (FEA), which has been shown to provide reliable predictions for ECAP [Baik, Estrin, Hellwig, Jeong, Brokmeier and Kim (2003)]. Therefore ECAP is a good benchmark for testing new numerical approaches such as MPM. It also involves an additional difficulty in that complex contact conditions are present between the work piece and the tools. As will be seen in this paper it turns out that most of the contact algorithms currently implemented in MPM codes are not capable of simulating ECAP properly. Therefore a new strategy had to be developed and it is presented in section 2.2.

## 2.2 Multimaterial Contact Treatment in MPM

The MPM simulations used the generalized interpolation method (GIMP) and the open-source code NairnMPM [NairnMPM]. The material model for pure copper is described below. The walls were modeled as rigid material points and interactions between the wall and the copper were modeled by MPM contact methods. In brief, these methods involve multi-material or multi-grid methods where each material extrapolates to its own velocity field on the background grid. All nodal points that have more than one material are contact nodes and contact methods are used to adjust the nodal momenta to implement various contact mechanics. Here the contact was modeled as frictionless. It is easy to add friction or to implement alternative contact physics. It was found, however, that traditional MPM contact methods [Bardenhagen, Guilkey, Roessig, Brackbill, Witzel and Foster (2001)] were inadequate for ECAP simulations. Therefore, a new contact algorithm was developed. Besides solving the ECAP problem, it can be recommended as an improved contact method for all MPM simulations.

The principles for multi-material contact are outlined in ref. [Bardenhagen, Guilkey, Roessig, Brackbill, Witzel and Foster (2001)]. Assuming that only two materials,  $a$  and  $b$ , interact (and all these simulations had only two materials - the walls and copper), a contact node will have extrapolated nodal velocities for each material,  $\vec{v}_a$  and  $\vec{v}_b$  and a normal vector,  $\hat{n}$ , defined as positive when directed from material  $a$  to material  $b$ . First define  $\Delta\vec{p}_a = \vec{p}_c - \vec{p}_a$  as the momentum change required for material  $a$  to change its momentum,  $\vec{p}_a$ , to the center-of-mass momentum,  $\vec{p}_c$ , on that node (note that most MPM codes track nodal momenta rather than velocity with velocities being calculated only when needed). The nodal velocity difference can be calculated from  $\Delta\vec{p}_a$ :

$$\vec{v}_b - \vec{v}_a = \Delta\vec{v} = \frac{m_a m_b}{m_a + m_b} \Delta\vec{p}_a, \quad (1)$$

where  $m_a$  and  $m_b$  are the nodal masses for materials  $a$  and  $b$  respectively. In addi-

tion, a tangent vector can be found that is tangent to the normal vector and in the direction of sliding motion:

$$\vec{t} = \Delta\vec{p}_a - (\Delta\vec{p}_a \cdot \hat{n})\hat{n}. \quad (2)$$

This vector may be zero, when there is no sliding motion, or may be normalized to a unit vector, when there is sliding motion. The first step of MPM contact is to detect the contact. A necessary, but not sufficient, criterion for contact is  $\Delta\vec{v} \cdot \hat{n} < 0$ , which implies the materials are moving towards each other. This condition is necessary, because otherwise contact methods would imply negative contact forces. It is not sufficient because this condition alone detects contact too soon (*i.e.*, before approaching surfaces are actually in contact). Various MPM methods have been tried for more accurate contact detection, such as surface stresses [Bardenhagen, Guilkey, Roessig, Brackbill, Witzel and Foster (2001)] or total nodal volume (J. E. Guilkey, personal communication, 2010). Here a new method was implemented based on extrapolated material positions. Contact was assumed to occur when both the velocity condition above is satisfied and when

$$\Delta\vec{u} \cdot \hat{n} = (\vec{u}_b - \vec{u}_a) \cdot \hat{n} < 0.8 \text{ cells}, \quad (3)$$

where material positions on the nodes are found by the usual MPM grid extrapolation methods:

$$\vec{u}_i = \frac{\sum_p m_p \vec{u}_p S_{ip}}{\sum_p m_p S_{ip}}, \quad (4)$$

where the sums are over all material points of one material type,  $m_p$  is the material point mass,  $\vec{u}_p$  is its position, and  $S_{ip}$  is the shape function for material point  $p$  on node  $i$ . The cutoff of 0.8 times the background cell dimension was found by calculations using GIMP shape functions with two materials exactly in contact. It is 0.8 rather than 0.0 due to the nature of boundaries in any particle based method; many tests showed that this criterion detects contact accurately.

Once contact is detected, the nodal momenta are adjusted to implement the chosen contact physics [Bardenhagen, Guilkey, Roessig, Brackbill, Witzel and Foster (2001)]. The momentum change required to move material  $a$  to the center-of-mass velocity field implies normal and tangential contact forces of

$$f_n = -\frac{\Delta\vec{p}_a \cdot \hat{n}}{\Delta t}$$

and

$$f_t = \frac{\Delta \vec{p}_a \cdot \vec{t}}{|\vec{t}| \Delta t} (\text{or } 0 \text{ if } |\vec{t}| = 0), \quad (5)$$

where  $\Delta t$  is the time step. Both of these forces are guaranteed to be positive (or zero) for all contact situations. For frictionless contact, the force  $-f_n$  is applied to material  $a$  in the normal direction, but no force is allowed in the tangential direction. The final momentum change applied to material  $a$  to model frictionless contact is

$$\Delta \vec{p}_a^* = (-f_n \Delta t) \hat{n}. \quad (6)$$

It is easy to implement Coulomb friction by comparing  $f_t$  to  $\mu f_n$ , where  $\mu$  is the coefficient of friction, and applying appropriate momenta changes for slip or stick conditions [Bardenhagen, Guilkey, Roessig, Brackbill, Witzel and Foster (2001)]. All simulations here used frictionless contact because FEA for ECAP had numerical problems when friction was turned on; our goal of comparing MPM to FEA was therefore limited to frictionless simulations. It is interesting to note that accounting for friction in FE simulations is difficult but should be straightforward in MPM. This issue will not be investigated further in the present paper but will be addressed in a future work.

These simulations had contact with rigid walls. If material  $a$  is the copper specimen and material  $b$  is the rigid wall, rigid contact was implemented by considering the walls to have infinite mass. In this limit, the rigid material velocity defines the center of mass velocity which leads to  $\Delta \vec{p}_a = m_a \vec{v}_b - \vec{p}_a$  and  $\Delta \vec{v} = \Delta \vec{p}_a / m_a$  where  $\vec{v}_b$  is the tracked rigid material velocity (this velocity was zero in all these simulations). All other contact methods are identical to deformable material contact, except that the position of the rigid walls is found by volume-weighted averaging instead of mass-weighted averaging (see Eq. (4)) and no momentum change is applied to the rigid walls. The inclusion of rigid particles in MPM code can be done conveniently by setting the mass of the rigid particles to their volume.

Both contact detection and changes in momenta depend on the surface normal. The usual practice for finding this normal is to handle each material separately with relation to the center-of-mass conditions. Thus the normal is found from the mass gradient of the current material [Bardenhagen, Guilkey, Roessig, Brackbill, Witzel and Foster (2001)]. This approach, however, was found to give very poor results. It also does not conserve momentum if two contacting materials have different mass gradients [Bardenhagen, Guilkey, Roessig, Brackbill, Witzel and Foster (2001)]. Therefore a new method was needed. First, during the MPM phase to extrapolate mass to the grid, mass-weighted shape function gradients were also extrapolated.

Due to nature of MPM extrapolation, this extrapolated gradient can be shown to be the negative of the mass gradient at node  $i$  or

$$\sum m_p \nabla S_{ip} = -\nabla m_i. \quad (7)$$

The new contact method implemented here was to take the surface normal vector as:

$$\vec{n} = \max \left( \frac{\nabla m_a}{\rho_a}, \frac{\nabla m_b}{\rho_b} \right). \quad (8)$$

The normal unit vector is found by normalizing  $\vec{n}$ . In other words, the normal vector was taken from the material whose volume gradient (from mass over density) has the largest magnitude. The volume gradient is needed instead of mass gradient to account for contact between materials with different densities or between deformable and rigid materials (if rigid material points have their mass equal to their volume, their density is set to 1 for the above equations). This new method for finding normals was found to improve simulations for a wide variety of contact problems, including the ECAP simulations. It also conserves momentum because each material in a contact pair will use the same normal.

One additional refinement was found to provide further improvement for the ECAP simulations. The rigid particles in the ECAP simulation are stationary and the volume gradient at contact nodes near these particles will give an exact result for the surface normals. Thus, in this special case the normals calculated from the rigid materials should be preferred over the volume gradient from the deformable material, whose volume gradient will fluctuate, particularly in regions of high deformation. We thus introduced a “rigid bias” factor,  $R_b$ , and found the contact normal from

$$\vec{n} = \max \left( \frac{\nabla m_a}{\rho_a}, R_b \frac{\nabla m_b}{\rho_b} \right). \quad (9)$$

In other words, the normal is taken from the rigid material unless the volume gradient for the deformable material is  $R_b$  times higher. Most simulations used  $R_b = 10$ . A finite  $R_b$  is preferred over an infinite value to protect against nodes with near-zero gradient from the rigid material. The numerical results below show examples of using conventional MPM contact and the new approach with either  $R_b = 1$  or  $R_b = 10$ .

### **3 Numerical models of ECAP**

All simulations were plane-strain calculations for ECAP processing of a rectangular rod with dimensions of 12x60 mm. The finite element analysis (FEA) was

conducted using the commercial package MSC-Marc. The die and plunger were assumed rigid and contact without friction was adopted in all simulations. In the finite element model, the rigid tools were described analytically by a set of curves, whereas in the MP model material points were used to define the geometry of the rigid entities. Details of the model setup are provided Fig. 2.

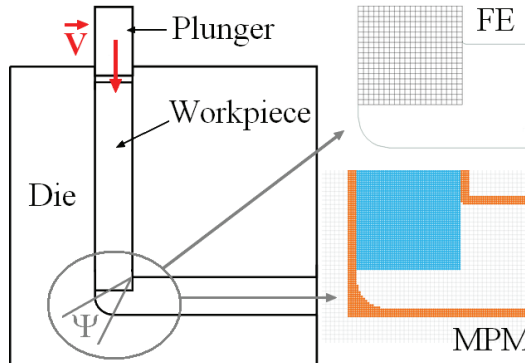


Figure 2: Diagram showing the 2D model of ECAP. A close up view is shown both for the FE and the MPM to emphasize the difference in discretization between the two methods.

### 3.1 Material model and parameters of pure copper

It has been shown that the microstructural evolution of copper can be accurately predicted by means of a dislocation-based model in which the material can be represented as a two-phase “composite” material consisting of dislocation cell walls with a large dislocation density and dislocation cell interiors relatively free of dislocations [Baik, Estrin, Hellmig, Jeong, Brokmeier and Kim (2003)]. Such a detailed analysis at the microstructure level is essential if the objective is to analyze the mechanisms of grain refinement with severe straining. In the present case however, our goal is to assess the suitability of a numerical method to simulate the mechanical process and therefore it was not deemed necessary to adopt this type of microstructure-based modeling. In fact, this could be detrimental since numerical problems associated with the subtleties of the material model itself, which involves the resolution of two coupled differential equations for the estimation of the dislocation densities, could introduce additional differences between the two numerical schemes.

Therefore the following simplified modeling approach was adopted for the constitutive behavior of copper. During the first pass of ECAP, an initially unstrained

copper billet experiences significant strain hardening. This strain hardening behavior is expressed by a power-law equation to estimate the flow stress evolution with plastic strain as follows:

$$\sigma_0 = A (\varepsilon_0 + \varepsilon^p)^n. \quad (10)$$

In this equation, the material parameters  $A$ ,  $\varepsilon_0$  and  $n$  were obtained from a numerical fit of experimental tensile data.

After subsequent passes of ECAP the material has undergone significant grain refinement which in turn leads to a saturation in yield stress, denoted  $\sigma_y^{fin}$ . Therefore a perfect plastic model with no strain hardening adequately represents the material flow stress after several passes. Here the level of saturation was adopted according to available data on copper processed by ECAP.

To summarize, two types of materials have been considered, namely pure copper exhibiting strain hardening and pure copper without strain hardening. These two distinct material behaviors are representative of an initially unstrained specimen and a specimen processed by several passes of ECAP, respectively. This analogy with the one pass/multiple passes situation has limitations. Indeed, only the representation of the flow stress is modified between the two cases, without any reference to the actual microstructure. Therefore important information such as residual stresses or initial texture are not accounted for in our model. Thus any direct comparison with experimental data, particularly in the ‘multiple passes’ case, should be interpreted with caution. To avoid any confusion, we will refer to the two constitutive behaviors as copper with strain hardening (Cu\_sh) and perfectly-plastic copper (Cu\_pp) respectively. The numerical values for the material parameters used in all subsequent simulations are provided in Tab. 1.

Table 1: Material parameters representative of pure copper used in this work.

E (MPa)	$\nu$	$\rho(\text{g.cm}^{-3})$	A (MPa)	$\varepsilon_0$	n	$\sigma_y^{fin}$ (MPa)
124000	0.33	8.96	260	0.013	0.37	400

#### 4 Preliminary numerical analyses

In this section the effect of several numerical parameters are investigated and discussed. First, since a quasi-static process is simulated by means of a dynamic explicit solver, it is crucial to ensure that any spurious inertial effects are minimized. Moreover, as in any finite element based model, the numerical solution is

affected by the resolution of the grid. Finally a comparison between different possible strategies for handling contact boundary conditions between the billet and the die walls is discussed.

#### 4.1 Calibration of the numerical plunger velocity

Since the momentum equations are solved using a dynamic explicit algorithm in NairnMPM, a small time step is typically required to ensure convergence. While this approach is well suited for the analysis of dynamic problems, under quasi-static conditions (as in the present case) a strategy must be adopted to minimize the total simulation time. Experimentally, the plunger moves at speeds of 4-10 mm/min. In our simulations a larger (fictitious) velocity was prescribed to reduce the total computing time. Of course, in doing so, undesirable inertial effects may perturb the overall solution. Therefore several simulations were conducted at different speeds to determine an optimum value for this simulation loading velocity.

The effect of plunger velocity was investigated by monitoring the normal component of the stress tensor along the direction of pressing and averaged over the whole sample. This scalar quantity will be denoted  $\sigma_{yy}$  in what follows. Fig. 3 shows  $\sigma_{yy}$  as a function of the plunger displacement recorded at three different speeds.

At the highest speed of 10 m/s, dynamic effects are clearly noticeable in the form of large oscillations in the global stress, particularly pronounced in the first 5 mm of the plunger displacement. During the first 2 mm of displacement, the work piece is simply pushed by the plunger thus the initial impact is accommodated in this phase. The angular extrusion itself only begins when the specimen comes in contact with the lower left corner of the die, after 2 mm of translational displacement. The inset within Fig. 3 is a close up of the first part of the deformation, from the moment the lower left part of the copper billet begins to deform plastically. At 2 m/s, important oscillations are still observed initially but these oscillations are quickly damped out after about 4 mm. The solutions obtained at a speed of 2 m/s and 0.5 m/s are in excellent agreement from 5 mm onwards, indicating that the solution has converged to the quasi-static limit. Since at 0.5 m/s no significant perturbation was observed throughout the simulation, this speed was considered adequate to reproduce the quasi-static solution and was used in all subsequent simulations. It should be noted that using an artificially large processing speed is only valid if the material is rate and temperature independent (as was assumed in our simulations). When using more realistic material models, this approach will lead to erroneous results therefore a different methodology must be adopted to reduce the simulation time.

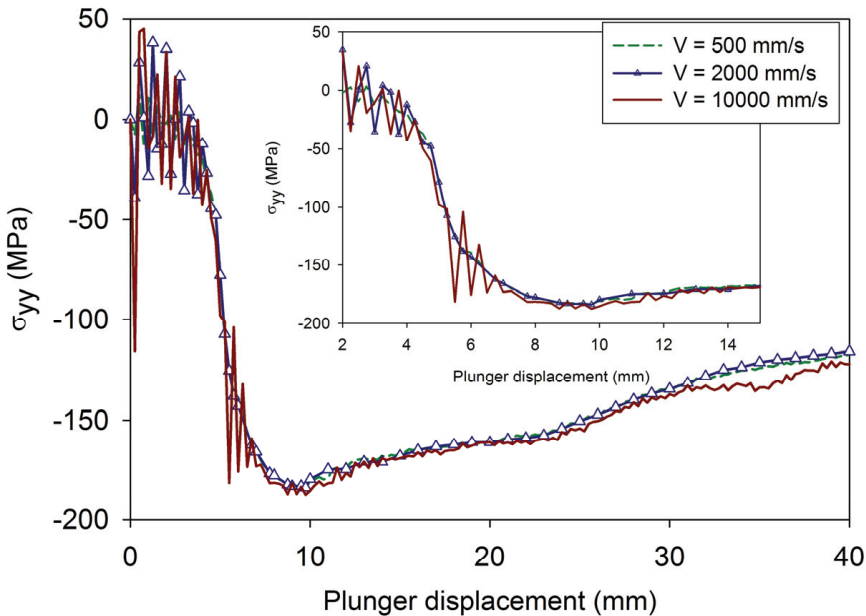


Figure 3:  $\sigma_{yy}$ , normal component of the stress tensor along the direction of pressing and averaged over the whole sample, as a function of plunger displacement as calculated at three different plunger speeds. The inset is a close up view of the left graph to more clearly display the first instants of pressing. In this test, Cu\_sh was selected and  $\Psi$  was set to 20 degrees.

#### 4.2 Sensitivity to spatial resolution

The next step was to determine spatial resolution requirements for accurate simulations. Our initial MPM calculations indicated that the overall shape of the extruded billet was strongly dependent on spatial resolution. Therefore the final specimen geometry was used as an indicator for spatial convergence. In particular, the final shape was characterized by two areas associated with local detachment of the work piece from the die. The specific location of these two detachment surfaces is indicated in Fig. 4. These areas, denoted here as A and B, are situated next to the lower left and lower right corner of the extruded specimen, respectively (see Fig. 4).

In FEM calculations, the contour of the work piece is clearly defined by the contours of the Lagrangian finite element mesh. The material interfaces in MPM, as with any particle-based method, are less clear. To solve this problem, the following procedure was adopted. During the simulation, each particle tracked both total

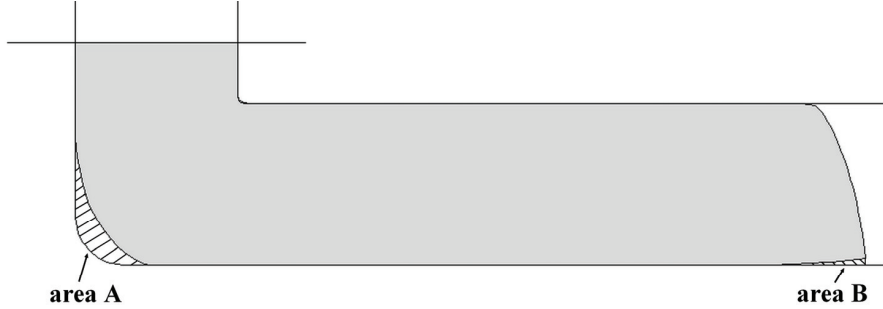


Figure 4: Definition of areas A and B corresponding to the formation of gaps between the work piece and the die, and used as indicator for spatial convergence of the numerical solution.

strain and total rotation strain, which can be combined to provide its deformation gradient. In post processing, the initial space-filling square material points were transformed and plotted using their deformation gradient. The resulting plot fills space well and allows for direct observations of material boundaries. Gaps between particles will open due to numerical accuracy and the gaps may get larger at higher deformations. In these simulations, however, the edges around areas A and B could be determined. Fig. 5 shows the variation of areas A and B as a function of grid size estimated both from FEA and MPM.

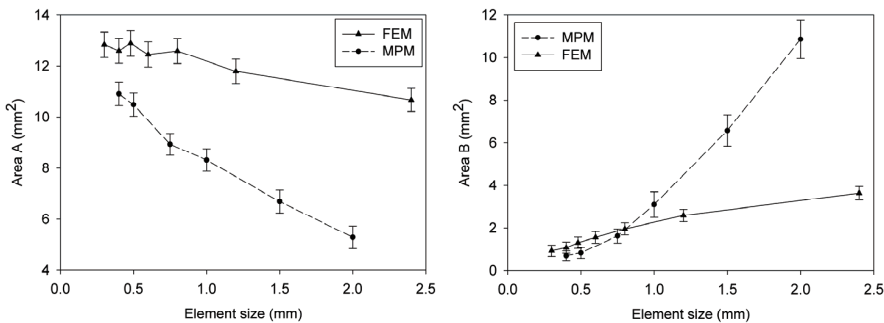


Figure 5: Variation of areas A and B (see Fig. 4) as a function of grid size. The error bars indicate an estimated standard uncertainty multiplied by a coverage factor of 2, corresponding to a 95 % level of confidence. Adjacent measurements are connected by straight lines to enhance the readability of this graph.

The results show that the solution deteriorates more rapidly in MPM than in FEM as the grid become coarser. On finer and similar grids (for an element size of approximately 0.8 mm and below), MPM and FEM give comparable estimates of area B and both converge to about 0.8-0.9 mm<sup>2</sup>. The prediction of area A by MPM and FEM are both trending to a limit value of about 13 mm<sup>2</sup>. However, assuming that this extrapolation is valid, MPM would require a much finer grid size to obtain the same level of accuracy as FEM, which in turn would be detrimental in terms of the required computing time. Refining the grid size from 0.5 mm to 0.4 mm already implies an increase in the total simulation time by a factor of 2.5 for a change in the estimated area A no greater than 4 %. Therefore, a compromise between precision and time efficiency was used. In the present work, grid sizes of 0.5 mm and 0.6 mm were chosen for the MPM and the FE model, respectively. With these resolutions, the FE model can be considered to give a reliable solution, while the MPM model exhibits a good trade-off between accuracy and execution time. Furthermore, the difference in MPM and FE predictions is between 8% and 30% for area A, while it is at most 3% for area B.

#### ***4.3 Role of the contact algorithm in the context of MPM simulations***

The new contact algorithm implemented in the current version of NairnMPM was described above. Here we consider simulations using three different contact methods:

- Conventional MPM contact [Bardenhagen, Guilkey, Roessig, Brackbill, Witzel and Foster (2001)] where normals are calculated from mass gradient of each material, in ECAP, that means from the deformable copper material.
- A revised method where normals are found from material that has the highest volume gradient.
- A revision specific to ECAP where normals are from the rigid material unless the deformable copper material volume gradient is  $R_b = 10$  times higher than the volume gradient for the rigid walls.

The results for equivalent plastic strain half way (50 ms) through three simulations with Cu\_sh are in Fig. 6. Fig. 6A shows that conventional MPM contact is very poor. The problems began when the corner of the billet encountered the corner of the channel. The calculation gets poor normals here which translated into inaccurate forces. The errors propagate along with the simulation. The simulation is greatly improved in Fig. 6B which used the new method with  $R_b = 1$ . This simulation still had artifacts near the initial contact point, which propagated along as an over-strained region. Furthermore the area B at the end of the billet did not agree

well with FEM simulation methods. Fig. 6C shows the optimal contact method for ECAP by using  $R_b = 10$ . This result had no artifacts and area B matched FEM well. All subsequent simulations in this study used this contact method. A key finding is that although MPM can implement complex contact easier than FEA, the contact mechanics can give poor results if the normals are not calculated well. Prior work on MPM contact has not addressed the importance of the contact normals.

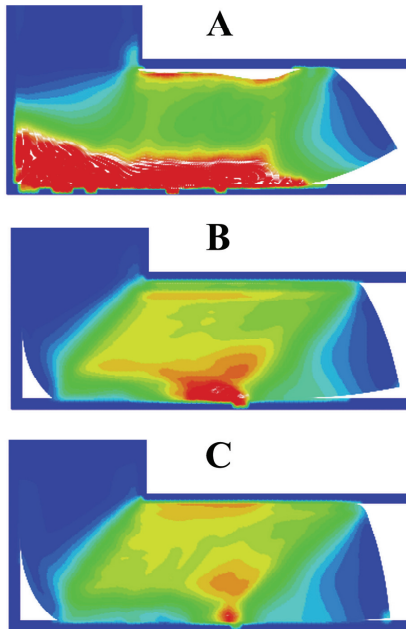


Figure 6: Three figures with the three contact methods listed above. Results are for Cu<sub>sh</sub>, they plot equivalent plastic strain on scale of 0 to 1.5. The results are at 50 ms.

## 5 Assessment of numerical MPM simulations of ECAP

Having calibrated the relevant numerical parameters for ECAP modeled by MPM, we then ran a series of MPM simulations for ECAP under different conditions. These results were compared to both FE simulations and previously reported results. As stated in the introduction, FEA has been shown to faithfully reproduce the ECAP experiments. Therefore the FE solution was used as the solution of reference in the present comparison. Nevertheless, it was also necessary to confirm

the consistency of our simulations by systematically referring to data from the literature, whenever a direct comparison was possible.

As has been explained in section 3, two different constitutive behaviors were considered, namely copper with strain hardening (denoted Cu\_sh) and perfect plastic copper (denoted Cu\_pp). For each copper material, three different angles for the outer die corner  $\Psi$  were considered, namely 1, 20 and 45 degrees. Thus, six different simulations were conducted.

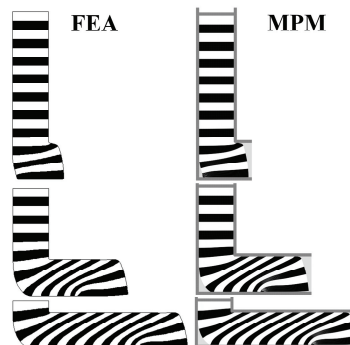


Figure 7: Deformation of Cu\_sh (copper with strain hardening) extruded in a 1 degree  $\Psi$  angle ECAP die. FE results (left) are shown side by side with MPM results (right) at 10 ms, 50 ms and 90 ms, from top to bottom respectively.

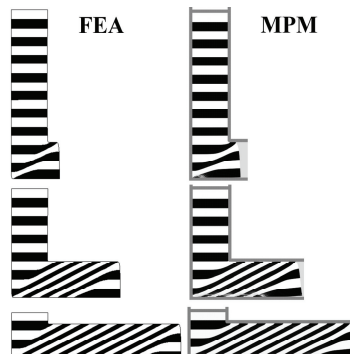


Figure 8: Deformation of Cu\_pp (copper with no strain hardening) extruded in a 1 degree  $\Psi$  angle ECAP die. FE results (left) are shown side by side with MPM results (right) at 10 ms, 50 ms and 90 ms, from top to bottom respectively.

### 5.1 Overall deformation behavior

Fig. 7 shows the deformed shape of the billet at three instants of an ECAP pass on Cu\_sh (copper with strain hardening). The angle  $\Psi$  was set to 1 degree in these simulations. Both results from MPM simulations and FEA are shown for comparison. Fig. 8 shows similar results obtained on Cu\_pp (copper with no strain hardening).

Comparing MPM and FE solutions, it is clear that both methods produce very similar results in terms of the deformed shape of the work piece as well as its internal deformation patterns. The most noticeable difference can be seen in the extrusion of Cu\_pp. In this case, the FE solution seems to be closer to the ideal simple shear loading, which is translated by straight and parallel internal strata oriented at a specific angle. In addition, the overall specimen shape is not significantly altered after extrusion. In contrast, the MPM solution in this case exhibits a more pronounced bended region at the far right end of the specimen, as well as more curved internal strata near the top and bottom die walls. These differences were attributed to the implementation of plastic laws in MPM, as will be discussed in more detail below.

The present results also agree well with existing data from the literature. Indeed on the 10 ms snapshot in Fig. 7 the transient deformation leading to the formation of a corner gap between the specimen and the die is identical to the numerical simulations performed under similar conditions by [Simsir, Karpuz and Gur (2010)] also using the FE code MSC-Marc. Moreover, the formation of this corner gap is only observed for a material exhibiting strain hardening behavior, an observation which is also consistent with previously reported numerical simulations [Kim, Seo and Hong (2000)]. The final orientation of the internal colored layers was estimated to be  $27 \pm 0.2$  degrees and  $29.9 \pm 0.8$  degrees with respect to the horizontal axis for Cu\_pp and Cu\_sh, respectively. A theoretical model of ECAP was described by [Beyerlein and Tóth (2009)] that gives an orientation of 26.6 degrees for a perfect plastic material, in accordance with our simulations. It should be noted that a direct quantitative comparison with experimental data is difficult since our current model does not incorporate the effect of friction, which is known to play an important role in the overall specimen deformation. Therefore the above observations on the corner gap formation as well as on the internal flow near the edges of the die are expected to differ experimentally. However, it is important to bear in mind that the present analysis aims at assessing the potential of MPM to simulate processes such as ECAP, acknowledging that several simplifying assumptions have been made in the model.

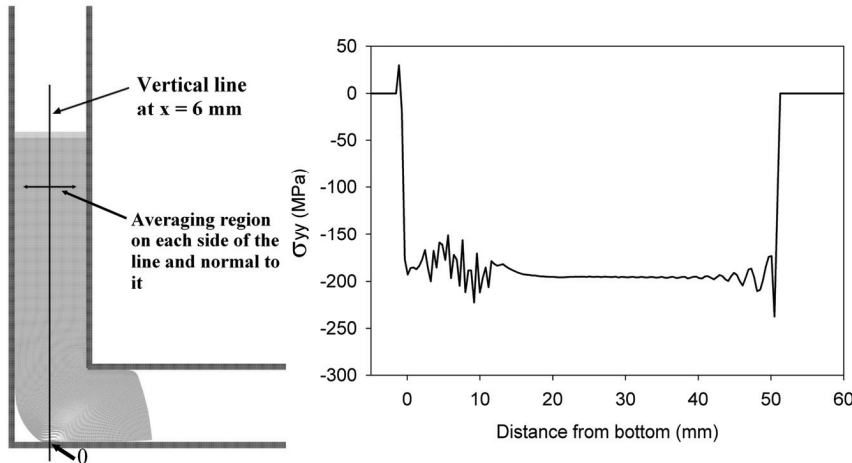


Figure 9: Left: The normal stress  $\sigma_{yy}$  was estimated on a vertical line running through the middle of the specimen and averaged on either side of the line and normal to it. Right:  $\sigma_{yy}$  calculated at 20 ms for Cu\_sh and  $\Psi = 1$  degree.

## 5.2 Punch load

Fig. 9 shows the normal stress  $\sigma_{yy}$  calculated along a vertical line positioned at  $x = 6$  mm (corresponding to the middle of the work piece) and averaged on either side of the line and normal to it. In order to avoid any edge effects, the stress was averaged over a  $\pm 5$  mm region, rather than over the full  $\pm 6$  mm width of the channel.

From Fig. 9 it is apparent that the normal stress calculated near the plunger displays important oscillations. These oscillations are still noticeable up to 10 mm below the plunger. Further away from this region and above the shearing zone, the stress is rather homogeneous and  $\sigma_{yy}$  is constant. Therefore the force exerted on the copper specimen can be estimated by taking an averaged value of the stress in the homogeneous area thus avoiding any edge effects close to the plunger.

Figs. 10 to 12 show the force exerted by the plunger as a function of its displacement for each angle  $\Psi$  and for both MPM and FE simulations. In post-processing, the force predicted by FEA is readily available on the rigid plunger. To estimate the same force in MPM, the normal stress  $\sigma_{yy}$  is averaged on a line located 20 mm below the plunger (averaging over a distance of  $\pm 4$  mm), to minimize the edge effect near the plunger described in the preceding paragraph.

Overall an excellent agreement is observed between MPM and FE simulations,

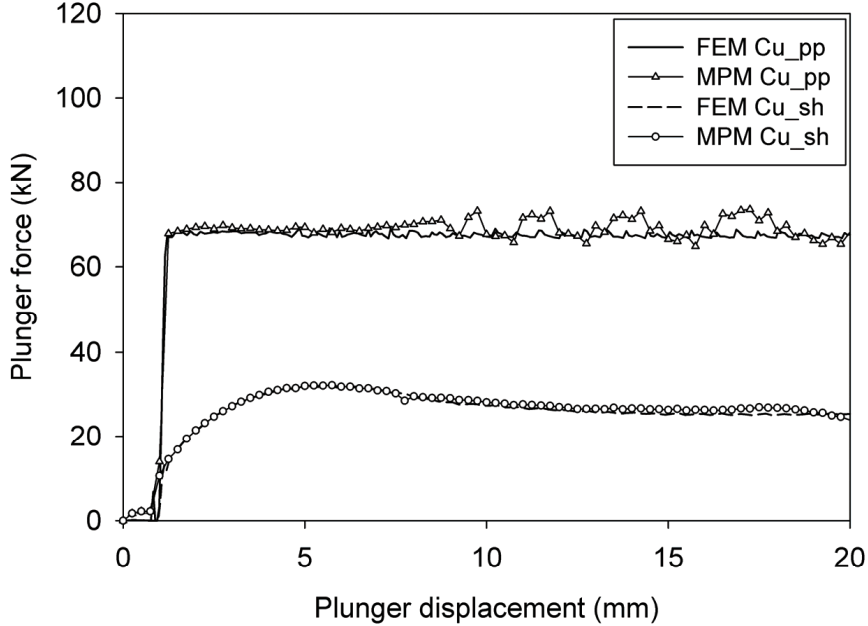


Figure 10: Estimation of the force exerted on the specimen as a function of the plunger displacement with a 1 degree  $\Psi$  angle configuration. Results for both Cu\_sh and Cu\_pp as calculated by MPM and FEA are shown.

especially on copper with strain hardening (Cu\_sh) for which the two sets of results are almost identical. Simulations conducted on Cu\_pp tend to produce a smoother force by FEA compared to MPM, as evidenced by spurious occasional oscillations on the MPM curves, which may be related to the specific location chosen to find the force. Nevertheless, the two methods match both in terms of the magnitude of the force as well as on its temporal evolution during an ECAP pass.

Compared to previous work, our simulations agree with reported data using a similar ECAP setup [Xu, Zhao, Ren and Ma (2008)]. Again, a direct quantitative comparison with experiments is not possible since no friction was accounted for in our model. Therefore we expect that our model would underestimate the actual experimental load. Our simulations show that the larger the corner angle, the smaller the required force to extrude the sample, in accordance with earlier reports [Balasundar, Rao and Raghu (2009)].

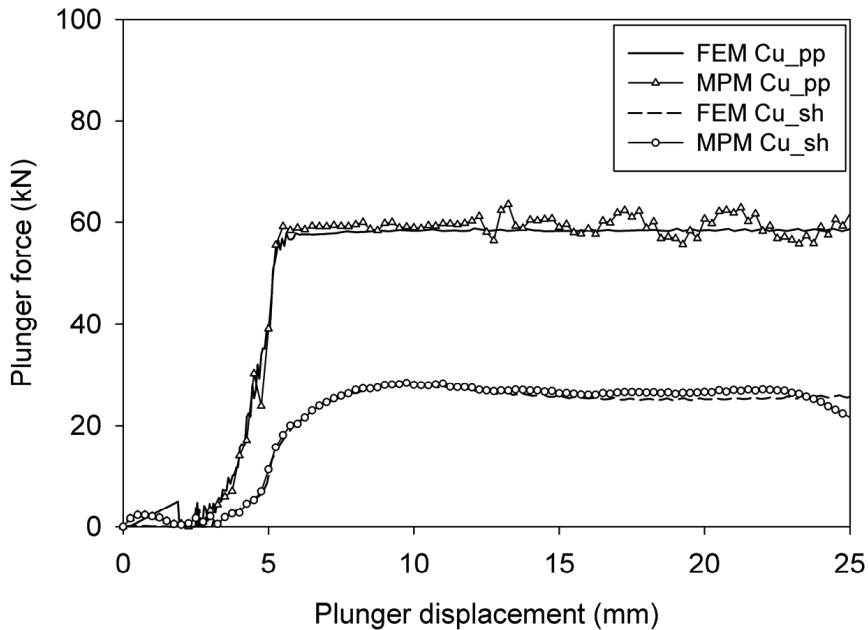


Figure 11: Estimation of the force exerted on the specimen as a function of the plunger displacement with a 20 degree  $\Psi$  angle configuration. Results for both Cu\_sh and Cu\_pp as calculated by MPM and FEA are shown.

### 5.3 Plastic strains

Having discussed the results in terms of global deformation patterns and global extrusion force, the local plastic strain field is now analyzed. Fig. 13 and 14 display the distribution of the equivalent plastic strain in the sample with MPM and FE results compared side by side in the case of Cu\_sh and Cu\_pp, respectively.

In almost all cases, the strain field calculated by MPM and FEA agree remarkably well. The only discrepancy can be seen on Cu\_pp extruded on a 1 degree angle die (Fig. 14, top image). In this case, MPM largely overestimates the plastic strains within the highest-strain region near the bottom of the die. This specific configuration combines a perfect plastic material with sharp die corners and is the most challenging to simulate because it generates relatively large strains (1.1 and above) in an extended area throughout the width of the sample. In all other cases, most of the deformation is limited to about 1 at most, except in localized regions where the specimen may experience larger strains. The material constitutive behavior in

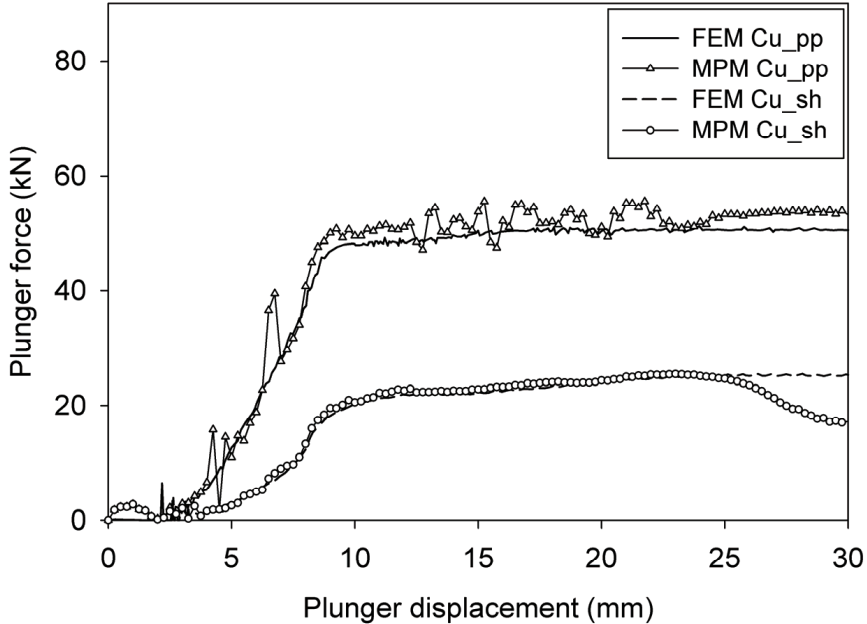


Figure 12: Estimation of the force exerted on the specimen as a function of the plunger displacement with a 45 degree  $\Psi$  angle configuration. Results for both Cu\_sh and Cu\_pp as calculated by MPM and FEA are shown.

NairnMPM is not formulated in its present form in the context of large inelastic deformations, although fairly large shear deformations are handled reasonably well. Therefore whenever a material is subjected to very large deformations, the MPM results are expected to overestimate the strains and lose accuracy in strain and stress fields. This issue has nothing to do with MPM, but is just a limitation of Nairn-MPM software used in this work. This limitation of NairnMPM will be addressed in future work by implementing a finite deformation formulation for elasto-plastic materials.

A material exhibiting strain hardening (Fig. 13) experiences a more pronounced strain gradient between the top and bottom tool walls as  $\Psi$  increases. This agrees with ref. [Xu, Zhao, Ren and Ma (2008)] in which a more homogeneous distribution was found when a smaller outer angle was selected. It is also interesting to note that earlier simulations conducted under similar frictionless conditions showed a comparable strain field, including in areas with localized higher strains (see ref.

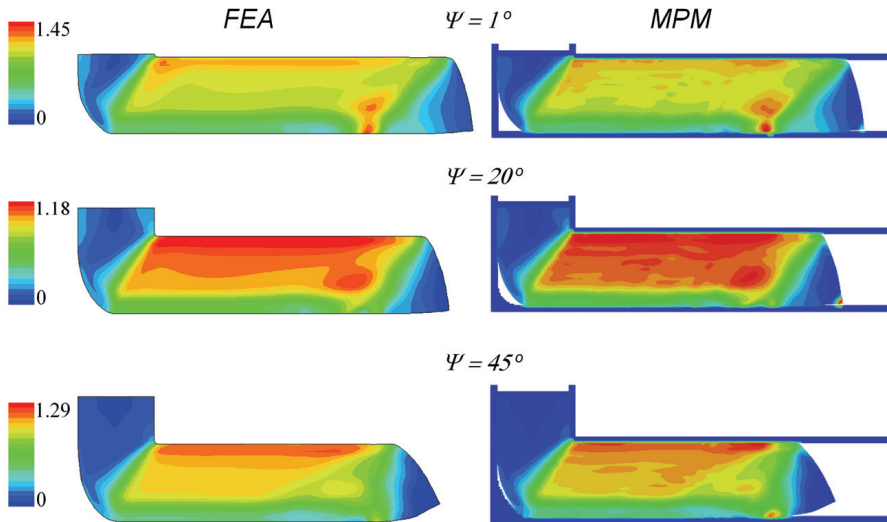


Figure 13: Equivalent plastic strain field at  $t=97$  ms for Cu\_sh simulated by MPM (left) and FEM (right). From top to bottom: outer angle  $\Psi$  of 1, 20 and 45 degrees respectively.

[Figueiredo, Pinheiro, Aguilar, Modenesi and Cetlin (2006)] and top image in Fig. 13). Of course, friction will have a significant effect on the actual strain field, as emphasized by [Balasundar, Rao and Raghu (2009)].

As expected, a more homogeneous plastic distribution is observed with Cu\_pp (see Fig. 14). While the present simulations do not fully represent a multi-pass ECAP process, the saturation in stress nevertheless mimics the homogeneity that would be observed on a material processed by several consecutive passes. Again, as with Cu\_sh, the plastic strain field for a non hardening material is consistent with previously reported data obtained under similar conditions, see for example Fig. 5 in ref. [Perez (2004)] which compares with the middle image of Fig. 14.

## 6 Conclusion

The Material Point Method has been applied to the simulation of the ECAP technique, a well established and widely used SPD process. The main objective was to assess the suitability of MPM as an alternative to more conventional finite element approaches to simulate complex problems involving contact and material non linearity. First, our simulations have shown that the grid resolution plays an

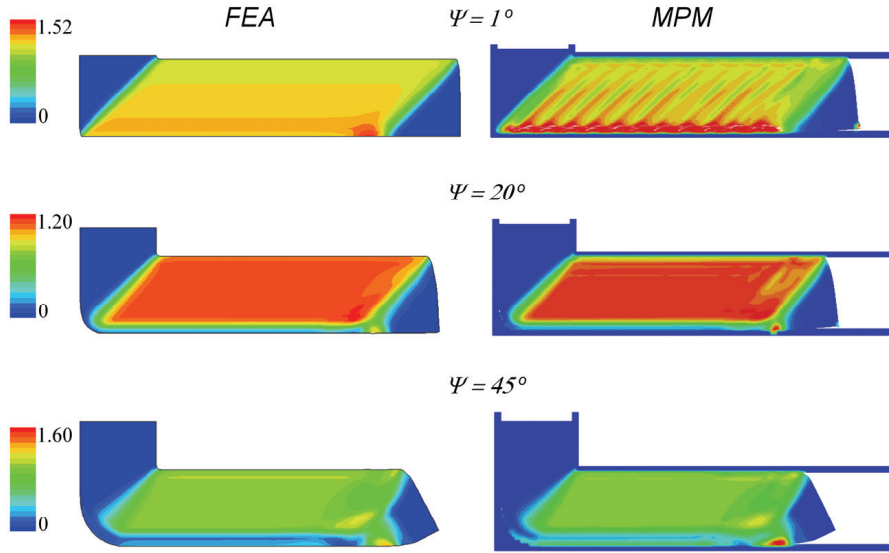


Figure 14: Equivalent plastic strain field at  $t=97$  ms for Cu\_pp simulated by MPM (left) and FEM (right). From top to bottom: outer angle  $\Psi$  of 1, 20 and 45 degrees respectively.

important role in the final accuracy of the numerical solution. The sensitivity to spatial resolution was clearly more pronounced than in the FE model. Second, this example demonstrates potential problems handling multi-material contact in MPM. MPM is often cited as having advantages for contact because contact can be modeled without the need for contact elements. This "contact-for-free" feature of MPM, however, is limited in accuracy unless the contact algorithm does an excellent job of tracking contact-surface normals. Here a new and general algorithm for the treatment of contact conditions was proposed. Furthermore, it was shown that a problem-specific modification (the rigid bias parameter) improved the contact calculations further and was needed to get the most accurate simulations. A number of ECAP simulations were run, by considering the extrusion of two different materials, and also by modifying the outer die angle, a parameter known to influence the overall mechanical behavior observed during an ECAP pass. It has been demonstrated that MPM gives similar results to conventional FEA. Moreover, our simulations agreed well with existing data from the literature. It is therefore concluded that MPM is a valuable alternative to FEA whenever large strains are expected. Future work will include a formulation of the stress-strain constitutive

behavior to improve the accuracy of NairnMPM in this context, will model contact with friction, and will also incorporate microstructure based material modeling. With this improvement, it will be possible to approach a wide range of problems which are notoriously difficult to simulate with FEA, including the so-called SPD processes.

**Acknowledgement:** J.N acknowledges support by a grant from the US Department of Agriculture, Cooperative State Research, Education, and Extension Service (2008-35504-19227).

Most MPM simulations were performed using CSIRO supercomputing facilities provided by CSIRO Advanced Scientific Computing which is gratefully acknowledged.

V.L. acknowledges valuable collaboration with Prof. Yuri Estrin on the numerical modeling of SPD processes, which provided the impetus for the present study.

## References

- Azushima, A., Kopp, R., Korhonen, A., Yang, D. Y., Micari, F., Lahoti, G. D., Groche, P., Yanagimoto, J., Tsuji, N., Rosochowski, A., Yanagida, A.** (2008): Severe plastic deformation (SPD) processes for metals. *Cirp Annals-Manufacturing Technology*, 57, 716-735.
- Baik, Seung Chul, Estrin, Yuri, Hellmig, Ralph J, Jeong, Hyo-Tae, Brokmeier, H.-G., Kim, Hyoung Seop** (2003): Modeling of texture evolution in copper under equal channel angular pressing. *Zeitschrift fÄ¼r Metallkunde*, 94, 1189-1198.
- Balasundar, I., Rao, M. S., Raghu, T.** (2009): Equal channel angular pressing die to extrude a variety of materials. *Materials & Design*, 30, 1050-1059.
- Bardenhagen, S. G., Guilkey, J. E., Roessig, K. M., Brackbill, J. U., Witzel, W. M., Foster, J. C.** (2001): An improved contact algorithm for the material point method and application to stress propagation in granular material. *CMES: Computer Modeling in Engineering and Science*, 2, 509-522.
- Bardenhagen, S. G., Brydon, A. D., Guilkey, J. E.** (2005): Insight into the physics of foam densification via numerical simulation. *J Mech Phys Solids*, 53, 597-617.
- Beyerlein, Irene J., Tóth, László S.** (2009): Texture evolution in equal-channel angular extrusion. *Prog Mater Sci*, 54, 427-510.
- Figueiredo, Roberto Braga, Pinheiro, Ivete Peixoto, Aguilar, Maria Teresa Paulino, Modenesi, Paulo JosÃ©, Cetlin, Paulo Roberto** (2006): The finite element analysis of equal channel angular pressing (ECAP) considering the strain path dependence of the work hardening of metals. *Journal of Materials Processing*

*Technology*, 180, 30-36.

**Kim, H. S.** (2001): Finite element analysis of high pressure torsion processing. *Journal of Materials Processing Technology*, 113, 617-621.

**Kim, H. S., Seo, M. H., Hong, S. I.** (2002): Finite element analysis of equal channel angular pressing of strain rate sensitive metals. *Journal of Materials Processing Technology*, 130, 497-503.

**Kim, Hyoung Seop, Seo, Min Hong, Hong, Sun Ig** (2000): On the die corner gap formation in equal channel angular pressing. *Materials Science and Engineering A*, 291, 86-90.

**Lapovok, R., Pougis, A., Lemiale, V., Orlov, D., Tóth, L., Estrin, Y.** (2010): Severe plastic deformation processes for thin samples. *Journal of Materials Science*, 45, 4554-4560.

**Moresi, L., Dufour, F., Mühlhaus, H. B.** (2003): A Lagrangian integration point finite element method for large deformation modeling of viscoelastic geomaterials. *Journal of Computational Physics*, 184, 476-497.

**Moresi, L., Quenette, S., Lemiale, V., Mériaux, C., Appelbe, B., Mühlhaus, H. B.** (2007): Computational approaches to studying non-linear dynamics of the crust and mantle. *Physics of The Earth and Planetary Interiors*, 163, 69-82.

**NairnMPM**, <http://people.oregonstate.edu/~nairnj/>.

**Nairn, J. A.** (2006): Numerical simulations of transverse compression and densification in wood. *Wood Fiber Sci*, 38, 576-591.

**Nairn, J. A.** (2003): Material point method calculations with explicit cracks. *CMES: Computer Modeling in Engineering and Science*, 4, 649-663.

**Nairn, J. A.** (2007): Numerical implementation of imperfect interfaces. *Computational Materials Science*, 40, 525-536.

**Perez, C. J. L.** (2004): On the correct selection of the channel die in ECAP processes. *Scripta Mater*, 50, 387-393.

**Simsir, C., Karpuz, P., Gur, C. H.** (2010): Quantitative analysis of the influence of strain hardening on equal channel angular pressing process. *Computational Materials Science*, 48, 633-639.

**Sulsky, D., Chen, Z., Schreyer, H. L.** (1994): A particle method for history-dependent materials. *Computer Methods in Applied Mechanics and Engineering*, 118, 179-196.

**Sulsky, Deborah, Zhou, Shi-Jian, Schreyer, Howard L.** (1995): Application of a particle-in-cell method to solid mechanics. *Computer Physics Communications*, 87, 236-252.

**Valiev, R. Z., Langdon, T. G.** (2006): Principles of equal-channel angular pressing as a processing tool for grain refinement. *Prog Mater Sci*, 51, 881-981.

**Wieckowski, Z.** (2004): The material point method in large strain engineering problems. *Computer Methods in Applied Mechanics and Engineering*, 193, 4417-4438.

**Xu, S., Zhao, G., Ren, G., Ma, X.** (2008): Numerical simulation and experimental investigation of pure copper deformation behavior for equal channel angular pressing/extrusion process. *Computational Materials Science*, 44, 247-252.

**Zhilyaev, A. P., Langdon, T. G.** (2008): Using high-pressure torsion for metal processing: Fundamentals and applications. *Prog Mater Sci*, 53, 893-979.